Synergistic effects of cerium-containing bioactive glasses and apoptotic extracellular vesicles alleviate bisphosphonate-related osteonecrosis of jaw

Ling, Ziji; Guo, Songsong; Xie, Hanyu; Chen, Xinyu; Yu, Kui; Jiang, Hongbing; Xu, Rongyao; Wu, Yunong; Zheng, Kai

DOI
10.1016/j.apmt.2024.102177

Publication date
2024

Document Version
Final published version

Published in
Applied Materials Today

Applied Materials Today 38 (2024) 102177

Contents lists available at ScienceDirect

Applied Materials Today

journal homepage: www.elsevier.com/locate/apmt

Synergistic effects of cerium-containing bioactive glasses and apoptotic extracellular vesicles alleviate bisphosphonate-related osteonecrosis of jaw

Ziji Ling [a,b,c,1], Songsong Guo [a,b,c,1], Hanyu Xie [a,b,c], Xinyu Chen [d], Kui Yu [e], Hongbing Jiang [a,b,c], Rongyao Xu [a,b,c], Yunong Wu [a,b,c,*], Kai Zheng [b,c,*]

[a] Department of Oral and Maxillofacial Surgery, Affiliated Hospital of Stomatology, Nanjing Medical University, Nanjing, 210029, China
[b] Jiangsu Province Engineering Research Center of Stomatological Translational Medicine, Nanjing Medical University, Nanjing, 210029, China
[c] Jiangsu Key Laboratory of Oral Diseases, Nanjing Medical University, Nanjing, 210029, China
[d] The first clinical medical college of Nanjing Medical University, Nanjing Medical University, Nanjing, 210029, China
[e] Department of Bionanoscience, Kavli Institute of Nanoscience, Delft University of Technology, 2629 HZ Delft, The Netherlands

ARTICLE INFO

Keywords:
Chitosan
Bioactive glass
Cerium
Apoptotic extracellular vesicles
Osteonecrosis

ABSTRACT

Bisphosphonates (BPs) are commonly used to treat skeletal diseases. However, long-term use of BPs can lead to BP-related jaw bone necrosis (BRONJ), particularly in patients undergoing tooth extraction surgery. The treatment of BRONJ remains challenging due to the local inflammatory microenvironment. To address this issue, we developed catechol-conjugated chitosan-based hydrogels incorporating cerium-doped mesoporous bioactive glass nanoparticles (Ce-MBGNs) and apoptotic extracellular vesicles (ApoEVs). The hydrogels containing 1 wt % Ce-MBGNs demonstrated biodegradability and non-cytotoxicity. The incorporation of Ce-MBGNs did not significantly impact gelation and rheological behavior. By leveraging the effects of Ce-MBGNs on regulating macrophage polarization and ApoEVs on mediating macrophage chemotaxis, hydrogels containing 1 wt % Ce-MBGNs and 1 mg/mL ApoEVs were able to recruit inflammatory macrophages and promote their M2 polarization. The in vivo experiments using a Zometa (ZA)-induced mice BRONJ model revealed that the synergistic effects of Ce-MBGNs and ApoEVs enhanced M2 polarization while reducing M1 polarization. This resulted in improved mucosal healing, bone regeneration, and alleviation of osteonecrosis. Overall, our study offers a new strategy for BRONJ therapy by addressing the inflammatory environment. Catechol-conjugated chitosan-based hydrogels containing Ce-MBGNs and ApoEVs have demonstrated impressive potential in the alleviation of BRONJ.

1. Introduction

Bisphosphonate-related osteonecrosis of jaw (BRONJ) is a rare disease with severe complications, clinically characterized by the presence of necrotic bone in the maxillofacial region for more than 8 weeks with a history of bisphosphonates (BPs) treatment and without a history of head or neck radiation therapy [1,2]. Despite the risk of developing BRONJ, BPs continue to be widely used in clinical practice for treating metabolic bone diseases, such as osteoporosis and bone metastasis [3–8]. Current interventions for BRONJ include medication, hyperbaric oxygen therapy, and surgical treatment. However, these interventions have some limitations and disadvantages [9,10]. For example, medication treatments, which are commonly used in the early stage of BRONJ and as adjuvant therapy in later stages, may lead to drug resistance, lack specificity, or cause toxic effects on other organs [11,12]. Emerging evidence has revealed that the pathogenesis of BRONJ involves a sustained pro-inflammatory state and abnormal macrophage polarization [13,14]. Therefore, therapeutic strategies focusing on regulating macrophage polarization have been considered feasible and effective methods for the alleviation of BRONJ.

Bioactive glasses (BGs) are widely used biomaterials for tissue regeneration and nanomedicine due to their osteogenesis, angiogenesis, anti-inflammatory, and antibacterial activities [15,16]. Incorporating active ions can further modulate the biological performances of BGs [15,

* Corresponding authors at: Jiangsu Province Engineering Research Center of Stomatological Translational Medicine, Affiliated Hospital of Stomatology, Nanjing Medical University, Nanjing, 210029, China.
E-mail addresses: yunongwu@njmu.edu.cn (Y. Wu), kaizheng@njmu.edu.cn (K. Zheng).
[1] These authors contributed equally to this work.

https://doi.org/10.1016/j.apmt.2024.102177
Received 16 July 2023; Received in revised form 20 March 2024; Accepted 24 March 2024
Available online 4 April 2024

17,18]. Engineering the morphological and textural properties of BGs can also improve their performances, beneficial for various biomedical applications. Typically, mesoporous bioactive glass nanoparticles (MBGNs) with nanoscale particle size, mesopores, and large specific surface area can act as delivery platforms of biologically active ions and biomolecules, inducing synergistic effects toward enhanced therapeutic outcomes [19–21]. BGs have been reported for treating BRONJ by prompting osteogenesis and angiogenesis [22]. However, the pro-inflammatory state in BRONJ is still a hindrance to effective bone regeneration. Cerium (Ce) can change its oxidative state between Ce^{3+} and Ce^{4+} during redox reactions, serving as a therapeutic ion to improve the antioxidant and anti-inflammatory properties of BGs [23–26]. For example, Ce-doped MBGNs (Ce-MBGNs) have been shown to drive the pro-inflammatory phenotype of macrophages to the anti-inflammatory phenotype by scavenging reactive oxygen species (ROS) and regulating oxidative stress [25–27]. Based on the above rationale, Ce-MBGNs are expected to be a feasible tool for BRONJ treatment to alleviate bone necrosis by modulating macrophage polarization. However, it is still challenging for Ce-MBGNs to target distant macrophages around the tooth extraction socket, considering their limited sphere of influence in the local bone microenvironment.

Apoptotic extracellular vesicles (ApoEVs) are released from apoptotic cells and contain various cellular components such as microRNAs, mRNAs, DNAs, proteins, and lipids [28–30]. ApoEVs can promote the recruitment and engulfment of phagocytic cells, particularly macrophages [31,32]. The recognition and clearance of apoptotic cells by phagocytes play a crucial role in tissue homeostasis, immune regulation, and inflammation remission [33]. Previous research has demonstrated that macrophages are the primary target cells for ApoEVs, acting as important "eat-me" signals that facilitate the efferocytosis process and regulate macrophage function [34]. In the context of BRONJ, it has been observed that the recruitment of macrophages to the affected area is impaired, probably responsible for the limited effectiveness of current treatment approaches [35,36]. Therefore, ApoEVs in combination with Ce-MBGNs are expected to promote the recruitment of macrophages, resulting in more effectively regulated macrophage polarization in BRONJ.

In this study, we developed catechol-conjugated chitosan-based hydrogels containing ApoEVs and Ce-MBGNs to address the challenge of BRONJ treatment. Catechol-conjugated chitosan-based hydrogels have gained significant attention in biomedical applications due to their properties such as injectability, thermosensitivity, and tissue adhesion, making them suitable for various therapeutic purposes, including wound healing and bone regeneration [37]. These chitosan-based hydrogels are thus expected to be promising delivery platforms for therapeutic nanoparticles and biomolecules. By combining ApoEVs and Ce-MBGNs, we anticipated an enhanced recruitment of macrophages to the affected area. Simultaneously, the presence of Ce-MBGNs allowed for the modulation of macrophage polarization, thereby improving the efficiency of macrophages in the treatment of BRONJ. Considering the specific environment within the oral cavity characterized by moisture and frequent chewing, we loaded both ApoEVs and Ce-MBGNs into a temperature-sensitive chitosan-based hydrogel. The efficacy of the developed formulations was evaluated in vitro and in vivo using Zometa (ZA)-stimulated macrophages and the BRONJ mouse model. Our study demonstrated that the combined action of Ce-MBGNs and ApoEVs effectively alleviated BRONJ, highlighting the synergistic effect of these therapeutic components. These findings suggest a promising strategy for the alleviation of BRONJ using our designed formulations.

2. Materials and methods

2.1. Materials and reagents

Cerium (III) nitrate hexahydrate, hydrocaffeic acid (HCA), chitosan, N-(3-Dimethylaminopropyl)-N′-ethyl carbodiimide hydrochloride (EDC) and Pluronic F-127 (PF-127) were purchased from Sigma-Aldrich. NaOH, HCl and ethanol were purchased from Sinopharm (Beijing, China). α-MEM, DMEM, FBS were purchased from Gibco Invitrogen (Waltham, USA). Cell counting kit 8 (CCK8) was purchased from APExBIO (Houston, USA). PBS, D-PBS and dialysis membranes were purchased from Solarbio (Beijing, China). Zometa (ZA) was purchased from Novartis Oncology (East Hanover, USA). Transwell chamber was purchased from Costar Corning (Corning, USA). RIPA buffer, lipopolysaccharide (LPS), IL-4, Dil, DiO, DAPI, paraformaldehyde, goat serum, Bradford protein assay kit and Triton X-100 were purchased from Beyotime (Shanghai, China). Polyvinylidene Fluoride (PVDF) membrane was purchased from Millipore (Billerica, USA). F4/80, CD206, CD86, TNF-α, PI3K, Akt, p-Akt (Ser473), mTOR, p-mTOR (Ser2448) and β-Actin antibody were purchased from Cell Signaling Technology (Danvers, USA). FITC or Cy3 labeled secondary IgG and horseradish peroxidase-conjugated secondary antibody were purchased from Proteintech (Hubei, China). RNA extraction kit was purchased from Bioteke (Beijing, China). HiScript II Q Select RT SuperMix for qPCR and ChamQ Universal SYBR qPCR Master Mix were purchased from Vazyme (Nanjing, China).

2.2. Synthesis of Ce-MBGNs

As reported previously, Ce-MBGNs were prepared using a microemulsion-assisted sol-gel process and post-impregnation [26]. Briefly, binary MBGNs (nominal composition $70SiO_2$-30CaO, in mol %) were synthesized first as described previously [26]. The obtained MBGNs were then soaked in 0.2 M cerium nitrate ethanol solution at a concentration of 10 mg/mL under stirring for 24 h at 30 °C to incorporate Ce. Then the mixture was centrifuged to collect the nanoparticles and washed once with ethanol. After drying at 60 °C overnight, the collected precipitate was calcinated at 700 °C for 4 h to obtain Ce-MBGNs. MBGNs without Ce incorporation were prepared as a control for further experiments. The morphology and mesoporous structure of Ce-MBGNs were evaluated using field emission scanning electron microscope (SEM, Auriga, Zeiss, Germany) and transmission electron microscopy (TEM, Phillips CM30, Netherlands).

2.3. Synthesis of CHI-C

As reported previously, catechol-conjugated chitosan (CHI-C) was synthesized using EDC chemistry [38]. In brief, 0.5 g chitosan (70 % deacetylation) was dissolved in 50 mL HCl solution and the pH was adjusted to 5. Then, 591 mg of HCA was dissolved in chitosan solution. EDC (0.62 g) dissolved in deionized water and ethanol (1:1 v/v, 25 mL) was slowly added to HCA chitosan solution and the pH was adjusted to 5.4∼5.6 by adding 1 M NaOH or 1 M HCl. After 12 h of reaction under stirring, the materials were dialysis with membrane (MWCO: 12000-14000) against HCl solution (pH 5.0) for 2 d and deionized water for 6 h, with refresh of dialysate every 8 h. The obtained products were then freeze-dried for 2 d to obtain CHI-C.

2.4. Preparation of ApoEVs and Ce-MBGNs loaded CH/PF hydrogels

To prepare ApoEVs and Ce-MBGNs loaded CHI-C/PF-127 hydrogels, CHI-C was dissolved in pH 7.4 PBS (2 wt %) and then mixed with the same volume of 24 wt % PF-127 solution at 4 °C to obtain CHI-C/PF-127 (CH/PF) hydrogel with the final concentrations of 1 wt % CHI-C and 12 wt % PF-127. Ce-MBGNs (or MBGNs) and ApoEVs were added into CH/PF hydrogel at 1 wt % and 1 mg/mL concentrations and homogenized at 4 °C. The obtained hydrogel solution was freeze-dried for further physiochemical characterization. For the in vitro cell study, the hydrogel solution was gelled at 37 °C first. No washing steps were performed, ensuring the full encapsulation of nanoparticles and ApoEVs.

2.5. Physiochemical characterization, in vitro degradation, ApoEVs release, and ion release of hydrogels

The morphology of the freeze-dried hydrogels was analyzed using SEM (JSM-7900F, JEOL, Japan). Fourier-transform infrared spectroscopy (FTIR) analysis was carried out in attenuated total reflectance (ATR) mode by using the spectrophotometer Nicolet iS 10 (Thermofisher, USA) with a resolution of 0.5 cm^{-1} in the wavenumber range of 2000–525 cm^{-1}.

The rheological properties of CH/PF hydrogel with and without nanoparticles were evaluated using a rheometer MCR102 (Anton Paar, Austria) equipped with a temperature controller. Elastic modulus (G') and viscous modulus (G'') were recorded using 20 mm parallel plates with increasing temperature. A constant stress of 100 Pa was used for the measurement. The gelation temperature was recorded with the crossover point of G' and G''.

To test the in vitro degradation of CH/PF hydrogel with or without nanoparticles, 1mL composite hydrogel samples were gelled at 37 °C for 10 min and then immersed in 3 mL PBS (pH 6.8) with 5 mg/mL of lysozyme added at 37 °C. At each predetermined time point, the supernatants were removed and the precipitations were freeze-dried for weighing.

The ion release behaviors of MBGNs or Ce-MBGNs incorporated CH/PF hydrogels were evaluated in D-PBS. In short, 1 mL CH/PF hydrogels containing 1 wt % MBGNs or Ce-MBGNs were immersed in 4 mL D-PBS solution at 37 °C and shaken at 90 rpm for 7 d. At each predetermined time point, 3 mL supernatant was collected and 3 mL fresh D-PBS was replenished. The ion concentration of the supernatant was analyzed using Inductively coupled plasma-atomic emission spectrometry (ICP-AES, AGILENT 725-ES, USA), and the ApoEVs concentration was assessed by using the BCA method (Pierce™ BCA Protein Assay Kits, Thermo Scientific, USA).

2.6. Cell culture

Murine macrophage cell line RAW 264.7 was purchased from the Cell Bank of Type Culture Collection of the Chinese Academy of Sciences. The cells were cultured in DMEM containing 10 % fetal bovine serum (FBS) at 37 °C and 5 % CO_2. RAW 264.7 was incubated with 10 μM ZA, 100 ng/mL LPS, or 40 ng/mL IL-4 for 24 h to identify the macrophage phenotype. To prepare a conditioned medium for the treatment groups, the plain hydrogels, the hydrogels containing ApoEVs and the hydrogels containing Ce-MBGNs (1 wt/v %) were soaked in a complete medium at the volume ratio of 1:5 for 24 h. Ce-MBGNs were also soaked in complete medium at 1 mg/mL for 24 h to prepare the conditioned medium. The supernatant was then collected, filtered, and used as conditioned medium.

2.7. Isolation and characterization of ApoEVs

Cell lines MC3T3, VECs, LECs, and L929 were used to isolate ApoEVs. For apoptosis induction, α-MEM (for MC3T3) and DMEM (for VECs, LECs, and L929) supplemented with 10 % EV-free FBS were prepared. Apoptosis was induced via UV irradiation (150 mJ/cm^2) for 1 h followed by 24 h of culture, and then supernatants were collected. Supernatants were centrifugated at 800 *g* for 10 min and 2000 *g* for 10 min to remove cell debris and then centrifuged at 16000 *g* for 30 min to precipitate the ApoEVs. The collected ApoEVs were resuspended with PBS and quantified with the Bradford protein assay kit before use. The morphology of ApoEVs was observed by TEM. Briefly, ApoEVs particles were suspended in 1 % glutaraldehyde for 30 min and then dropped on the Formvar-coated copper grid for 20 min. The samples were then negatively stained with 2.5 % uranyl acetate for 2 min. The images were taken with TEM (JEM-1400Flash, JEOL, Japan).

2.8. Cell Counting Kit-8 (CCK-8) assay

A density of 1×10^3/well RAW 264.7 was seeded to a 96-well plate and cultured overnight. The original culture medium was removed, and a complete medium (control group) or conditioned medium was added to the well-plates. On the 1st, 3rd, 5th, and 7th day, culture medium was replaced with 100μL culture medium containing 10μL CCK8 solution. After incubation at 37°C for 2 h, the absorbance at 450 nm was measured for the supernatant of each well with an enzyme-linked immunosorbent assay reader (ELx800; BioTek Instruments, USA).

2.9. Macrophage recruitment and migration assay

In order to evaluate the influence of different apoptotic cells on the recruitment of macrophages, ApoEVs from different cell lines were added to the lower chamber of 8 μm Transwell chamber and 8×10^4 RAW 264.7 was added to the upper chamber containing serum-free medium. After the migration of cells for 24 h, the chamber was fixed with 4 % paraformaldehyde and then stained with crystal violet solution for 15 min. After being washed with PBS, the non-migrating cells on the inner membrane of the chambers were wiped off and the outer membrane was observed and images were taken under a microscope (Leica Microsystems, Mannheim, Germany).

2.10. Phagocytosis assay

To evaluate the ApoEVs of phagocytosis by macrophages, RAW 264.7 were seeded on coverslips overnight. ApoEVs were prelabeled with DiO according to the manufacturer's protocol and were added into RAW 264.7 and co-cultured for 3 h. Then the cells on the coverslips were labeled with Dil for 30 min, fixed with 4 % paraformaldehyde for 30 min and stained with DAPI for 90 s at room temperature. The images were captured using a fluorescence microscope (Leica Microsystems, Germany).

2.11. Cell immunofluorescence

RAW 264.7 cells were seeded on coverslips overnight to a density of 30 % and then cultured with complete medium or conditioned medium for 24 h. The cells on the coverslips were fixed with 4 % paraformaldehyde for 30 min and then infiltrated with 1 % Triton X-100. Goat serum was used to pre-incubate to block non-specific staining. The cells were incubated with the primary antibody overnight at 4°C, then washed with PBS and incubated with FITC or Cy3 labeled secondary IgG for 45 min at 37°C. The coverslips were labeled with DAPI for 90 s at room temperature. The images were captured using a fluorescence microscope.

2.12. Western blot (WB) analysis

RAW 264.7 cells were seeded into a 6-well plate at a density of 6×10^5/well and cultured overnight. After culture with complete medium or conditioned medium for 24 h, the cells were lysed in RIPA buffer containing phosphatase inhibitors and protease inhibitors. Then, the protein lysate was separated by SDS-PAGE, and transferred to a PVDF membrane. The membrane was blocked in 5wt % skim milk for 2 h and then incubated in the primary antibody overnight. After being washed 3 times with TBST, the membrane was incubated with the horseradish peroxidase-conjugated secondary antibody for 50 min. The WB was visualized by using ECL detection. Relative protein levels were quantified as the ratio of target protein levels to β-actin levels in each group.

2.13. Real-time quantitative PCR analysis

RNA extraction kit was used to extract total RNA from the cells following the instructions. Reverse transcription was performed using

HiScript II Q Select RT SuperMix for qPCR. Real-time quantitative PCR analysis was performed using ChamQ Universal SYBR qPCR Master Mix, and each set of experiments was repeated at least 3 times by Applied Biosystems Quantstudio 7 real-time PCR system (Thermo Fisher, USA). The level of each mRNA was standardized to GAPDH, and the relative quantification of gene expression was calculated using the $2^{-\Delta\Delta CT}$ method. The primer sequences used in this study are listed in Table 1.

2.14. Animal study

Twenty-five C57BL/6J male mice (6-week-old) were obtained from the Animal Center of Nanjing Medical University and raised by the SPF Experimental Animal Center of Nanjing Medical University. The animal experiments were approved by the Ethics Committee of Nanjing Medical University (Approval ID 2006014). The BRONJ model was induced by the tail vein injection of ZA (Zometa, Novartis Oncology, East Hanover, NJ, USA) 125 μg/kg twice a week and the control group was injected PBS instead. The animal experiments were divided into 5 groups: the control group (without ZA or materials), the ZA group, the plain hydrogel + ZA group, the hydrogel + Ce-MBGNs + ZA group, and the hydrogel + Ce-MBGNs + ApoEVs + ZA group. First, the maxillary molars of mice were extracted under deep anesthesia. After tooth extraction, the mice in the experimental groups were injected with different groups of materials near the periodontal area of the first molar. The injection of ZA was continued twice per week for 4 weeks, and then the mice were sacrificed and the samples were analyzed.

2.15. Micro-computed tomography (micro-CT) analysis

The micro-CT scanner (SCANCO Medical AG, Switzerland) was used to evaluate the micro-structural characteristics of the maxilla in mice. The mouse maxilla was dissected, and the excess soft tissue was removed before the micro-CT was performed. Maxillae were scanned with a high resolution of 18 μm and energy of 50 kV and 456 μA. NRecon v1.6 and CTAn v1.13.8.1 software were used to construct and analyze 3D images of bones. The area of interest was defined and focused on the alveolar bone of the mouse's maxillary first molar periodontal. The bone mineral density (BMD) and bone volume ratio (BV/TV) were calculated to analyze the bone structure.

2.16. Histological, immunohistochemistry and immunofluorescence staining

After being removed from the maxilla of the mouse, bone was fixed with 4 % paraformaldehyde for at least 24 h and decalcified with 10 % EDTA. After the samples were dehydrated and embedded, a paraffin microtome (Leica, Germany) was used to prepare 4-μm-thick sections for hematoxylin and eosin (H&E) staining.

For immunohistochemistry (IHC), after dewaxing using xylene and hydration with ethanol, the specimens were then subjected to heat treatment with sodium citrate in the boiling water bath for 20 min. Treatment with 3 % H_2O_2 followed for 20 min, and the sections were subsequently incubated with goat serum for 30 min at room temperature. Following this, the sections were incubated with TNF-α antibodies overnight at 4°C. After PBS washing, the sections were incubated with secondary antibodies at room temperature for 20 minutes and then subjected to 3,3′-Diaminobenzidine and hematoxylin staining.

For immunofluorescence (IF) staining, bone tissue was treated with antigen retrieval and incubated overnight with specific antibodies against macrophage markers (F4/80, CD86, or CD206) and then stained as previously described. The images were captured using a fluorescence microscope.

Table 1
Primer sequence of genes for qRT-PCR analysis

Genes	Primer sequence 5′- 3′ forward (F) and reverse (R)
GAPDH	F 5'-AACTTTGGCATTGTGGAAGG-3'
	R 5'-TGTGAGGGAGATGCTCAGTG-3'
INOS	F 5'-GTTCTCAGCCCAACAATACAAGA-3'
	R 5'-GTGGACGGGTCGATGTCAC-3'
TNF-α	F 5'-CCCTCACACTCAGATCATCTTCT-3'
	R 5'-GCTACGACGTGGGCTACAG-3'
IL-6	F 5'-TAGTCCTTCCTACCCCAATTTCC-3'
	R 5'-TTGGTCCTTAGCCACTCCTTC-3'
Arg1	F 5'-CTCCAAGCCAAAGTCCTTAGAG-3'
	R 5'-AGGAGCTGTCATTAGGGACATC-3'
TGF-β	F 5'-CTCCCGTGGCTTCTAGTGC-3'
	R 5'-GCCTTAGTTTGGACAGGATCTG-3'
IL-10	F 5'-GCTCTTACTGACTGGCATGAG-3'
	R 5'-CGCAGCTCTAGGAGCATGTG-3'

2.17. Statistical analysis

Statistical analysis was performed using GraphPad Prism 10 software. Student's t-test was used to assess the statistical significance of comparisons between the two groups. One-way ANOVA was performed for multiple comparisons. p values less than 0.05 (*), 0.01 (**) and 0.001 (***) were considered statistically significant. Experiments were independently repeated at least three times.

3. Results

3.1. Characterization of Ce-MBGN-containing CH/PF hydrogels

We first investigated the physiochemical properties of Ce-MBGNs and chitosan-based hydrogels containing these nanoparticles. Fig. 1A shows representative SEM and TEM images of Ce-MBGNs, which exhibited a mesoporous structure with a spherical shape and particle size between 100 and 200 nm, typical of nanoparticles synthesized using microemulsion-assisted sol-gel processing [26]. Our previous study confirmed the chemical composition of Ce-MBGNs to be 86.0 SiO_2-11.2 CaO-2.8 CeO_2 (mol %). Incorporating these nanoparticles into polymeric hydrogels could endow the hydrogel with antioxidant capacity [26]. Fig. 1B displays SEM images of freeze-dried CH, CH/PF, CH/PF + Ce-MBGNs and CH/PF + MBGNs hydrogels. CH hydrogels had porous surfaces with pore sizes ranging from ~100 to 300 μm after freeze-drying. CH/PF hydrogels also had porous surfaces but appeared to have smaller pores. After the incorporation of MBGNs and Ce-MBGNs, the surface structure of CH/PF hydrogels became denser, and fewer surface pores were observed (Fig. 1B). Despite this, the hydrogels containing nanoparticles still maintained a porous structure, as pores could be seen underneath the surface. Moreover, nanoparticles could be observed on the surface of hydrogels (as indicated in the yellow rectangles in Fig. 1B), indicating the successful incorporation of MBGNs.

Fig. 1C shows the FTIR spectra of CH, CH/PF, CH/PF + MBGNs, and CH/PF + Ce-MBGNs. The bands observed at 1159 and 1074 cm^{-1} corresponded to the vibrational modes of saccharide units and C-O and C-N stretching, respectively [38]. The band at 1056 cm^{-1} was attributed to Si-O-Si stretching [26]. These bands confirmed the successful combination of CH/PF and nanoparticles in CH/PF + MBGNs and CH/PF + Ce-MBGNs. Moreover, no new bands were observed after incorporating MBGNs and Ce-MBGNs, which suggested the non-covalent interaction between hydrogel molecules and nanoparticles. Rheological tests were performed to track the evolution of elastic modulus (G') and viscous modulus (G'') to monitor gel formation. The intersection points between G' and G'' were considered gelation points. As shown in Fig. 1D, the transition temperatures of CH/PF, CH/PF + MBGNs, and CH/PF + Ce-MBGNs were found to be 30.9, 29.2, and 28.6 °C, respectively. The presence of nanoparticles slightly reduced the gelation temperature of the hydrogels.

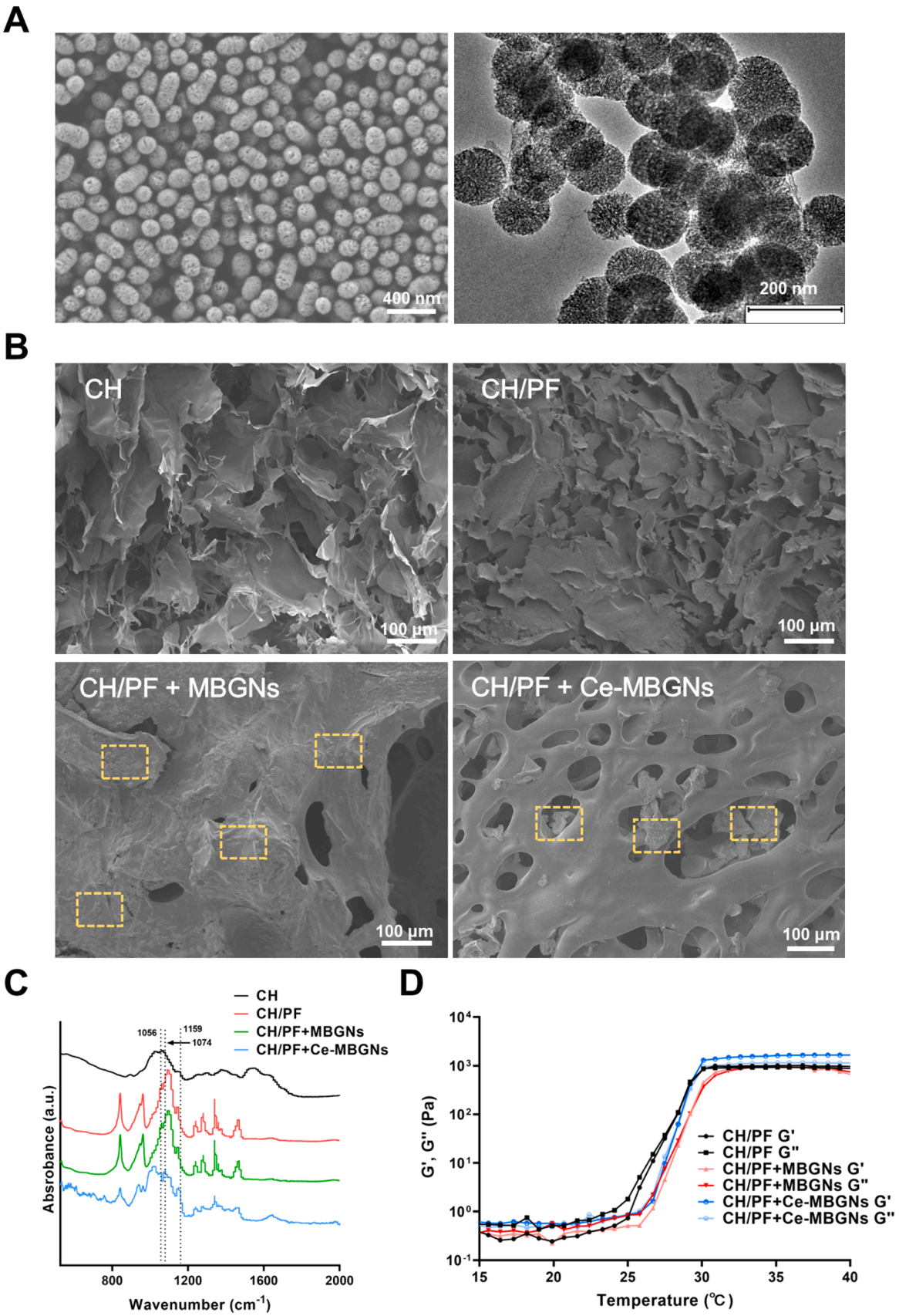

Fig 1. (A) Representative SEM and TEM images of Ce-MBGNs; (B) Representative SEM images of CH, CH/PF, CH/PF + MBGNs and CH/PF + Ce-MBGNs hydrogels after freeze-drying (The rectangles in yellow indicate the presence of the nanoparticles); (C) FTIR spectra of CH, CH/PF and CH/PF + MBGNs; (D) Elastic (G') and viscous (G'') modulus of CH/PF, CH/PF + MBGNs and CH/PF + Ce-MBGNs.

3.2. In vitro degradation and ion release behavior

To assess the degradation behaviors of the hydrogels, we analyzed their mass loss in a lysozyme-containing DPBS in vitro. Fig. 2A demonstrates that the majority of mass loss occurred during the first week, with only approximately 4 % mass loss observed in the subsequent two weeks. This limited mass loss in the later stages may be attributed to the high crosslinking degree of CH resulting from repeated lyophilization. The remaining mass percentages at 21 days were found to be 63, 56, 73, and 74 % for CH, CH/PF, CH/PF + MBGNs, and CH/PF + Ce-MBGNs, respectively. The presence of nanoparticles seemed to enhance the stability of the hydrogels in lysozyme-containing PBS. Compared to the MBGNs group, Ce-MBGNs did not significantly impact the degradation of the hydrogels. The release of ApoEVs from the CH/PF hydrogels is depicted in Fig. 2B. approximately 55 % of ApoEVs were initially released by all groups within the first 8 hours. Subsequently, at 24 and 72 hours, the CH/PF group demonstrated a higher release of ApoEVs compared to the CH/PF + MBGNs and CH/PF + Ce-MBGNs groups. By 168 hours, all three groups had released approximately 90 % of ApoEVs. Notably, no statistical differences were observed in the release behavior between the CH/PF + MBGNs and CH/PF + Ce-MBGNs groups. These results indicate that the CH/PF hydrogels can consistently release ApoEVs, with the initial release being slightly higher and potentially influenced by the specific characteristics and interactions of the hydrogels. Overall, the CH/PF hydrogels demonstrate sustained and stable release of ApoEVs over an extended period.

Fig. 2C illustrates the ion release behaviors of CH/PF + MBGNs and CH/PF + Ce-MBGNs in DPBS over 14 days. Both groups exhibited sustained and stable release of Ca ions, indicating that CH/PF hydrogels effectively sustained the ion release from both MBGNs and Ce-MBGNs. The release of Si ions from the MBGNs and Ce-MBGNs groups was similar, with no significant difference observed. Notably, no Ce ions were detected in the solution for either group.

3.3. ApoEVs promote the recruitment and migration of macrophage

We conducted a migration assay to evaluate the recruitment ability of ApoEVs from different cell lines to macrophages. Fig. 3A demonstrates that the largest number of cells migrated to the outer membrane in the MC3T3 group, indicating that the ApoEVs from MC3T3 have a stronger ability to recruit macrophages than those from VECs, LECs, and L929 cell lines. Based on this result, the ApoEVs from MC3T3 were selected as the macrophage chemotactic factor for subsequent experiments. We confirmed the size and morphology of isolated ApoEVs using TEM, as shown in Fig. 3B, in which ApoEVs exhibited a typical cup-shaped structure with a particle size of approximately 100 nm. We evaluated the phagocytic function of macrophages on ApoEVs using a phagocytosis assay. DiO-labeled ApoEVs were co-cultured with macrophages labeled with Dil and DAPI. Fig. 3C demonstrates that the DiO-labeled ApoEVs were successfully engulfed by macrophages, as evidenced by the co-localization of the red and green fluorescence.

3.4. Ce-MBGNs promote M2 polarization of macrophage

We employed the CCK-8 assay to assess the in vitro cytotoxicity of CH/PF hydrogel, ApoEVs, and Ce-MBGNs. As shown in Fig. 4A, no significant differences were observed in the OD values between the control group and all the conditioned media groups, indicating the non-cytotoxicity of CH/PF hydrogel, ApoEVs, and Ce-MBGNs. Additionally, all the groups exhibited similar proliferation trends over 7 days, suggesting that the CH/PF hydrogels, ApoEVs, and Ce-MBGNs did not have a noticeable adverse effect on the proliferation of RAW 264.7 cells.

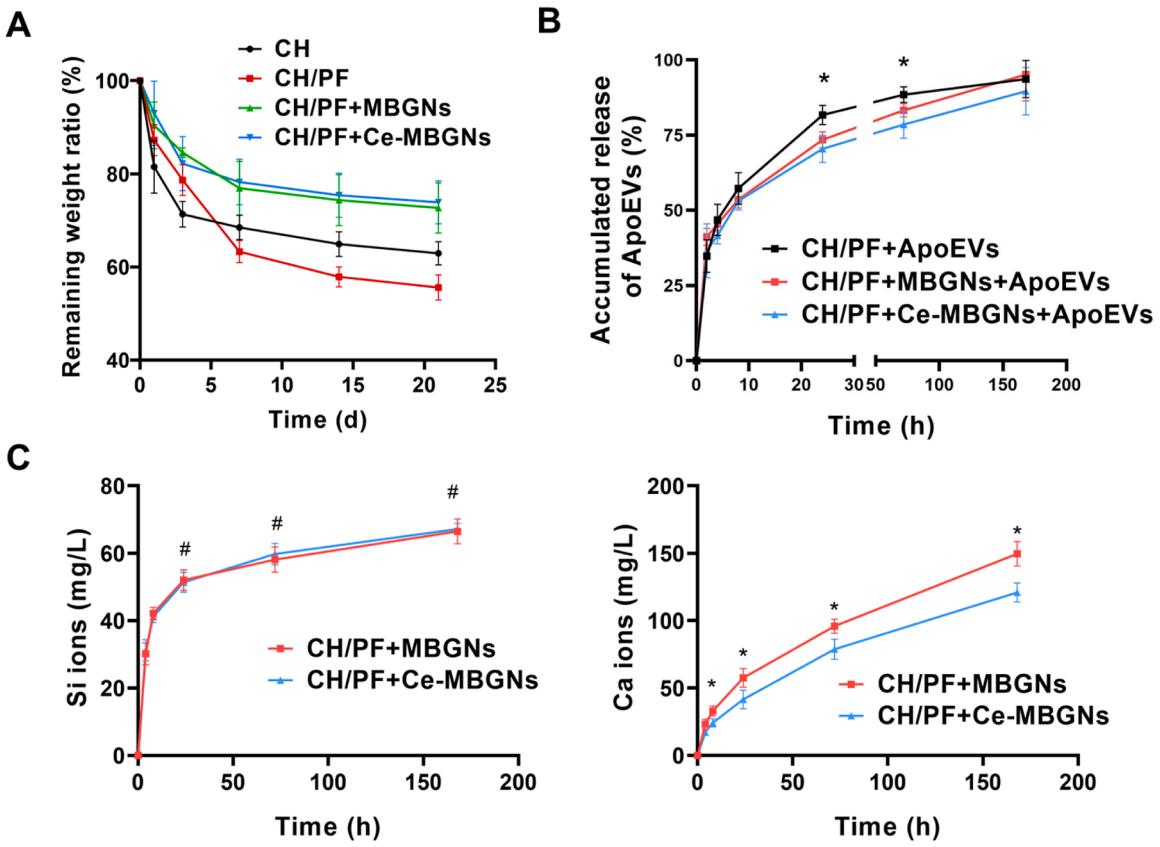

Fig. 2. Degradation and Ion release profiles of CH/PF with MBGNs or Ce-MBGNs. (A) In vitro degradation behaviors of CH, CH/PF, CH/PF + MBGNs and CH/PF + Ce-MBGNs. (B) ApoEVs release behaviors of CH/PF, CH/PF + MBGNs and CH/PF + Ce-MBGNs. (C) Si and Ca ion release behaviors of CH/PF + MBGNs and CH/PF + Ce-MBGNs. The experiment was performed in triplicates with three technical repeats. $p < 0.05$ (*) and $p > 0.05$ (#).

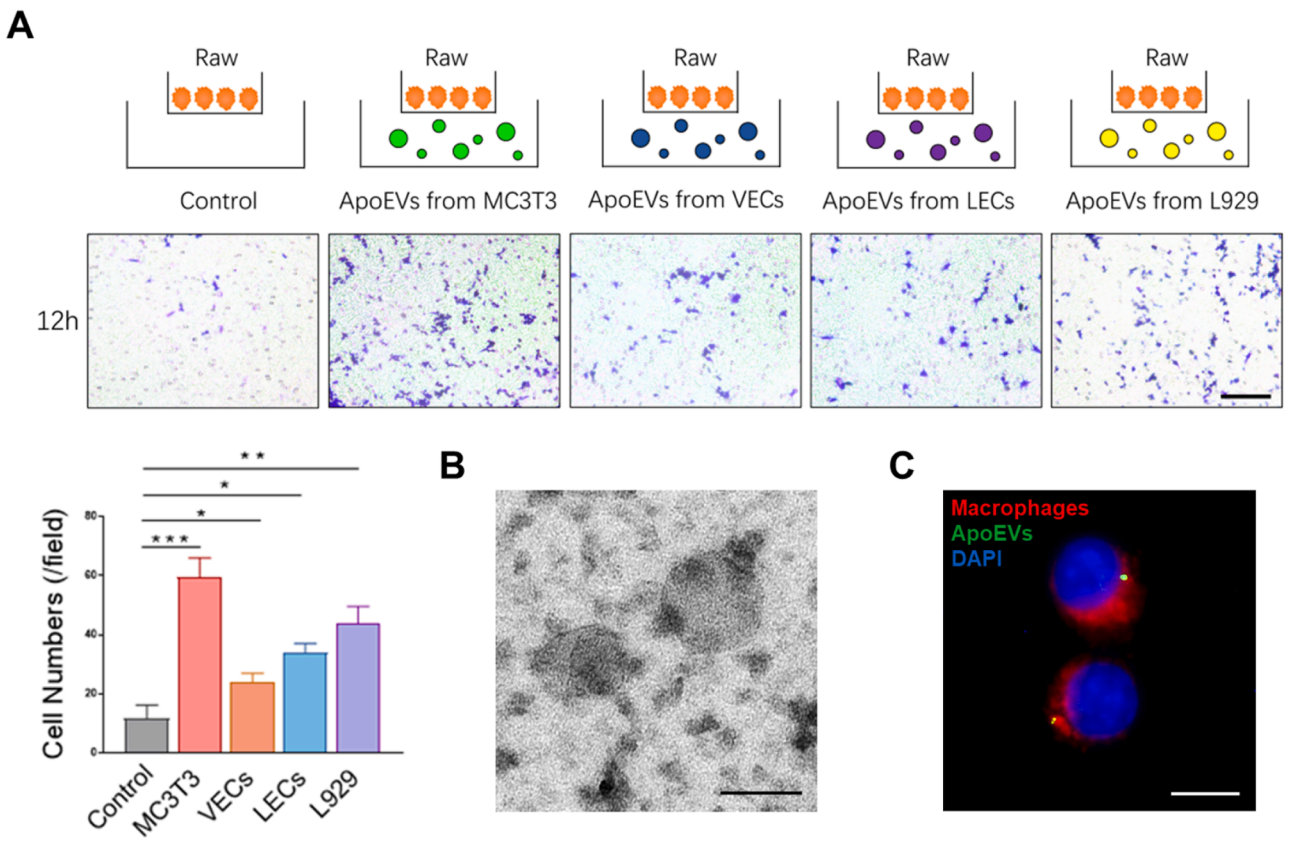

Fig. 3. ApoEVs promote the recruitment and migration of macrophages. (A) Migration assay of the recruitment ability of MC3T3, VECs, LECs, and L929' ApoEVs to the macrophage. Scale bar = 80 μm (B) TEM image of ApoEVs. Scale bar = 100 nm. (C) Phagocytosis assay showed the phagocytic function of macrophage on ApoEVs. ApoEVs were labeled with DiO (green), macrophages' plasma membrane was labeled with Dil (red), and macrophages' nuclei were labeled with DAPI (blue). Scale bar = 10 μm. The experiment was performed in triplicate independently with three technical repeats. $p < 0.05$ (*), $p < 0.01$ (**) and $p < 0.001$ (***).

We conducted cell immunofluorescence, WB, and qRT-PCR analyses to investigate the influence of ZA, Ce-MBGNs, CH/PF hydrogels, ApoEVs and their combinations on macrophage polarization. Fig. 4B shows the WB results and their quantitative analysis, in which CD86 and CD206 were used as markers for M1 and M2 macrophages, respectively. Treatment with ZA only led to increased expression of CD86 and decreased expression of CD206, while treatment with Ce-MBGNs only had the opposite effect on the expression of CD86 and CD206. CH/PF hydrogel alone and CH/PF + ApoEVs did not have significant influence on the polarization of macrophages. When ZA was loaded in CH/PF + ApoEVs hydrogels, they still increased the expression of CD86 and decreased the expression of CD206, although the extent was slightly reduced compared to ZA treatment only. Notably, when Ce-MBGNs were loaded in CH/PF + ApoEVs + ZA hydrogels, the composite hydrogels reversed the effects induced by ZA and significantly downregulated the expression of CD86 and upregulated the expression of CD206.

Furthermore, the qRT-PCR results in Fig. 4C show that ZA upregulated the expression of M1-related and pro-inflammatory cytokine genes, including iNOS, TNF-α, and IL-6, while downregulating the expression of M2-related and anti-inflammatory genes, including Arginase1, TGF-β1, and IL-10, as displayed in Fig. 4D. Compared to the ZA group, Ce-MBGNs significantly downregulated the expression of M1-related genes and upregulated the expression of M2-related genes. CH/PF hydrogel alone and CH/PF + ApoEVs hydrogels did not significantly affect pro-inflammatory and anti-inflammatory genes. When ZA was loaded into CH/PF + ApoEVs hydrogels, its effects on these genes were retained. Notably, the incorporation of Ce-MBGNs into CH/PF + ApoEVs + ZA hydrogels counteracted the effects induced by ZA.

Fig. 4E shows immunofluorescence results, and F4/80, CD86, and CD206 were used as markers for unstimulated macrophages, M1 macrophages, and M2 macrophages, respectively. Compared to the control, neither CH/PF hydrogels nor ApoEVs significantly affected macrophage polarization. ZA alone increased the M1 polarization ratio and decreased the M2 polarization ratio, while the addition of Ce-MBGNs resulted in a reduced M1 polarization ratio and an increased M2 polarization ratio. When ZA and Ce-MBGNs were incorporated into CH/PF hydrogels, their effects on M1 and M2 polarization were retained.

Given the pivotal role of the PI3K/Akt/mTOR signaling pathway in macrophage metabolism and polarization, we assessed the impact of ZA and Ce-MBGNs on this pathway. The WB results and their quantitative analysis (Fig. 4F) indicate that ZA stimulation increased Akt and mTOR phosphorylation compared to the blank control, while the hydrogels only and hydrogels + ApoEVs groups did not increase the Akt and mTOR phosphorylation. The hydrogels + ApoEVs + ZA increased Akt and mTOR phosphorylation compared to the control, though the extent was slightly lower than that induced by ZA. Notably, the Hydrogel + ZA + Ce-MBGNs + ApoEVs group did not increase Akt and mTOR phosphorylation compared to the blank control. Only the groups containing ZA could increase the Akt and mTOR phosphorylation.

3.5. Synergistic effects of ApoEVs and Ce-MBGNs on extraction socket healing in BRONJ model

To evaluate the therapeutic potential of ApoEVs and Ce-MBGNs in treating BRONJ, we conducted in vivo experiments using a mouse model. It should be pointed out that the extraction sockets of mice had been intravenously injected with ZA to develop the BRONJ model before the introduction of the hydrogel formulations, except for the control group (injection PBS only without ZA). The healing of mucosal and bone

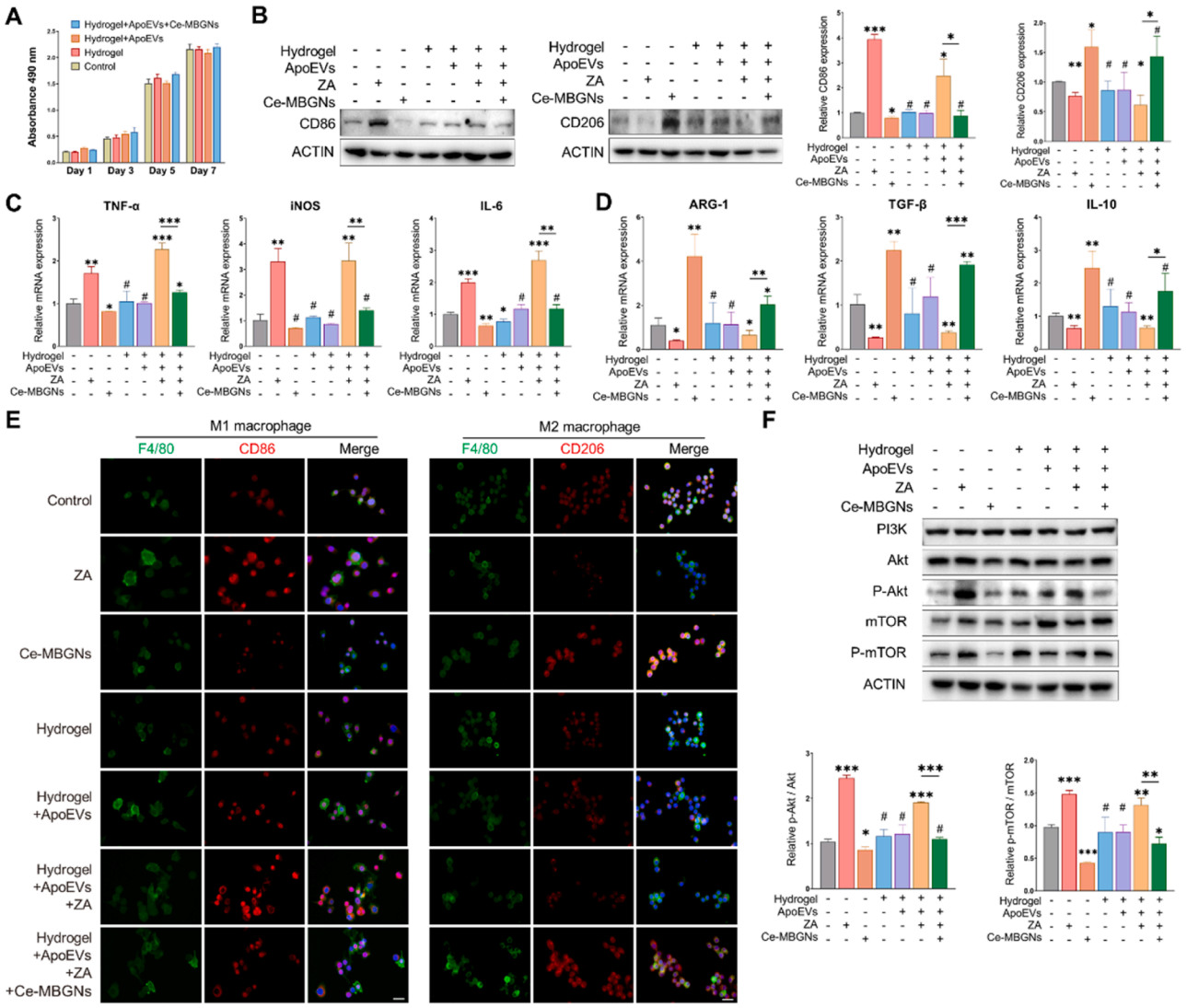

Fig. 4. (A) The CCK-8 assay results of macrophages cultured with the conditioned medium of hydrogel, ApoEVs and Ce-MBGNs. (B) WB results of macrophage stimulated by CH/PF hydrogel, ApoEVs, ZA, Ce-MBGNs and their combinations. (+) means the presence of the constituent; (-) means the absence of the constituent. Relative CD86 and CD206 levels normalized to β-Actin were expressed as fold-change. (C, D) The qRT-PCR results show the expression of pro-inflammatory cytokines genes (iNOS, TNF-α and IL-6) (C) and anti-inflammatory genes (Arginase1, TGF-β1 and IL-10) (D) after stimulated by CH/PF hydrogel, ApoEVs, ZA, Ce-MBGNs and their combinations. (E) Cell immunofluorescence results show the polarization of macrophages stimulated by CH/PF hydrogel, ApoEVs, ZA, Ce-MBGNs and their combinations. Scale bar = 20 μm. (F) WB results of PI3K/Akt/mTOR pathway stimulated by CH/PF hydrogel, ApoEVs, ZA, Ce-MBGNs and their combinations. The relative ratio of p-Akt/Akt and p-mTOR/mTOR were expressed as fold-change. The experiment was performed in triplicate independently with three technical repeats. $p < 0.05$ (*), $p < 0.01$ (**), $p < 0.001$ (***) and $p > 0.05$ (#).

exposure in the extraction sockets was observed, and gross analysis showed that the ZA and CH/PF hydrogel groups had delayed healing compared to the control group, while the CH/PF hydrogels contain Ce-MBGNs group and Ce-MBGNs + ApoEVs group significantly promoted the healing, close to the healing of the control. The number of mice with exposed sockets was lower in the Ce-MBGNs + ApoEVs and Ce-MBGNs groups than in ZA only and CH/PF hydrogel groups. The number of mice with exposed sockets in the Ce-MBGNs + ApoEVs group was lower than in the Ce-MBGNs group.

Micro-CT analysis (Fig. 5B) was performed to assess the bone mass, as BMD and BV/TV indicated. The results showed that the ZA only and hydrogel groups had significantly lower bone mass than the control. Although the hydrogel + Ce-MBGNs still had lower bone mass than the control, they had a higher bone mass than the ZA only and hydrogel groups. Hydrogel + Ce-MBGNs + ApoEVs group had a higher bone mass than the hydrogel + Ce-MBGNs group and its bone mass was close to that of the control. HE staining (Fig. 5C) revealed that the ZA only and CH/PF hydrogel groups had a significant increase in the necrotic bone area compared to the control group. The typical structure of osteonecrosis, empty osteocyte lacuna, could be seen in the ZA only group as indicated by arrows. These structures could also be observed in the other three groups. The number of empty osteocyte lacuna in the ZA+ hydrogel group was similar to that in the ZA group. Both Ce-MBGNs and Ce-MBGNs + ApoEVs groups had significantly lower numbers of empty osteocyte lacuna than the ZA and hydrogel groups. Furthermore, material residual was not observed in the HE staining results, which indicated the full degradation of hydrogel formulations after injection in vivo within 4 weeks.

We also performed an immunohistochemistry (IHC) of TNF-α to assess the inflammatory status in vivo. The results (Fig. 5D) showed that the TNF-α staining intensity was markedly increased in the ZA only and hydrogel groups compared to the control group. The Ce-MBGNs group exhibited a significantly lower extent of TNF-α staining compared to the ZA only and hydrogel groups. The combination of Ce-MBGNs and

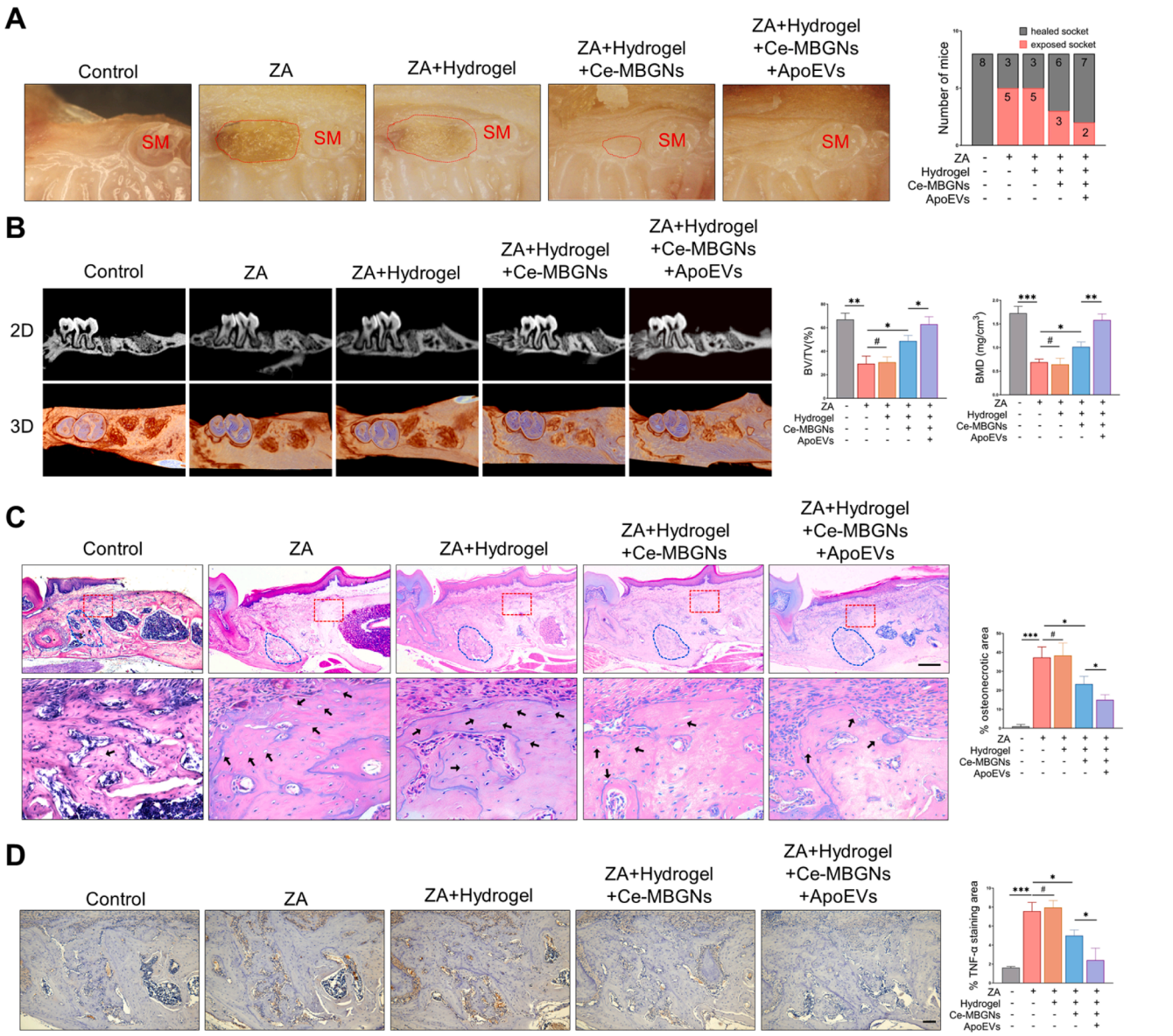

Fig. 5. ApoEVs and Ce-MBGNs promote the healing of extraction sockets in the BRONJ model. (+) means the presence of the constituent; (-) means the absence of the constituent. (A) Gross observation of healing of mucosal and bone exposure of extraction sockets in Control, ZA, hydrogel, Ce-MBGNs and Ce-MBGNs + ApoEVs groups. The red-marked area indicates an exposed bone surface with unhealed mucosa. SM: second molar. (B) Micro-CT analysis shows the bone healing of extraction sockets in Control, ZA, hydrogel, Ce-MBGNs and Ce-MBGNs + ApoEVs groups. (C) HE staining of the formed necrotic bone (red-marked area) and tooth extraction wound (blue-marked area) in Control, ZA, hydrogel, Ce-MBGNs and Ce-MBGNs + ApoEVs groups. Arrows indicate empty osteocyte lacuna; Scale bar = 1 mm. (D) IHC images of TNF-α and the proportion of positive areas in tooth extraction wounds of Control, ZA, hydrogel, Ce-MBGNs and Ce-MBGNs + ApoEVs groups. Scale bar = 100 μm. $p < 0.05$ (*), $p < 0.001$ (***) and $p > 0.05$ (#).

ApoEVs further reduced the TNF-α level, close to the control group. The results showed that using Ce-MBGNs and ApoEVs could significantly reduce the inflammatory status. Overall, our findings indicate that utilizing ApoEVs and Ce-MBGNs can effectively promote mucosal healing, reduce necrotic bone formation, and alleviate inflammation levels in the BRONJ model.

3.6. ApoEVs and Ce-MBGNs synergistically promote M2 polarization of macrophage in the BRONJ model

We conducted immunofluorescence experiments to investigate the influence of ApoEVs and Ce-MBGNs on macrophage polarization in the BRONJ model. The results (Fig. 6) demonstrated that the ZA group exhibited a significant increase in M1 macrophage polarization and a decrease in M2 macrophage polarization compared to the control group. In contrast, both the Ce-MBGNs group and Ce-MBGNs + ApoEVs group displayed a macrophage polarization phenotype characterized by reduced M1 macrophage polarization (Fig. 6A) and enhanced M2 macrophage polarization (Fig. 6B) compared to the ZA only and hydrogel groups. Furthermore, the Ce-MBGNs + ApoEVs group exhibited a more pronounced effect on macrophage polarization than the Ce-MBGNs group, indicating that ApoEVs and Ce-MBGNs possess a considerable capability to promote M2 macrophage polarization, which is associated with anti-inflammatory responses and tissue repair in the BRONJ model. These findings provide evidence for the immunomodulatory properties of ApoEVs and Ce-MBGNs in inducing a favorable macrophage phenotype in the context of BRONJ.

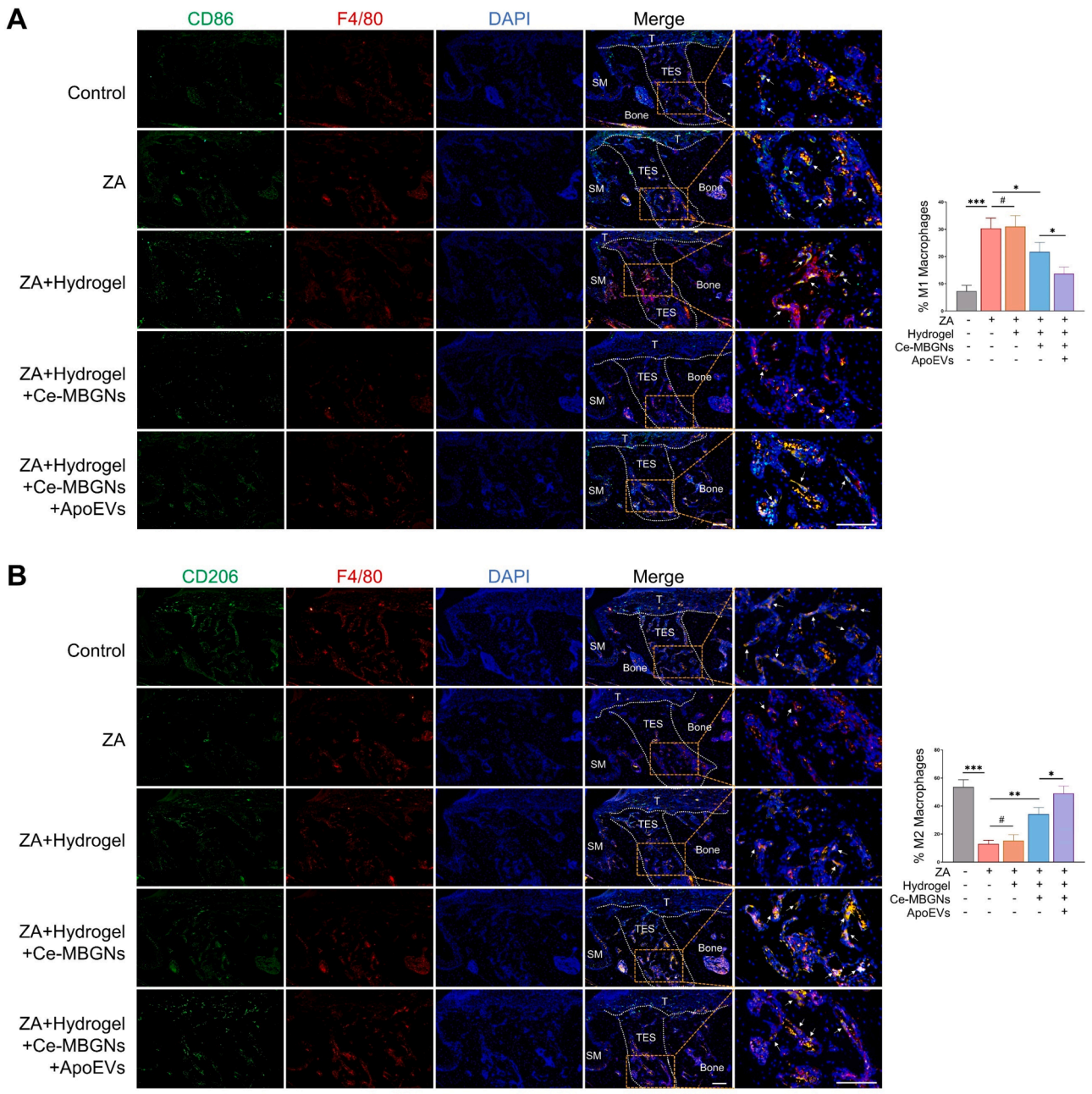

Fig. 6. ApoEVs and Ce-MBGNs promote macrophage M2 polarization in the BRONJ model. (+) means the presence of the constituent; (-) means the absence of the constituent. Immunofluorescence shows the M1 (A) and M2 (B) polarization of macrophages in Control, ZA, hydrogel, Ce-MBGNs and Ce-MBGNs + ApoEVs groups. The marked area in white indicates the tooth extraction socket (TES). The rectangles in yellow indicate the images with higher magnification. M1 or M2 macrophages are indicated by white arrows. SM: second molar. T: treated area shows the hydrogels have completely degraded and been replaced by epithelial structures. Scale bar = 1 mm. $p < 0.05$ (*), $p < 0.01$ (*) and $p > 0.05$ (#).

4. Discussion

Bisphosphonates (BPs) are commonly used to manage bone loss and bone metastasis due to their ability to inhibit bone resorption [1]. However, prolonged use of BPs increases the risk of developing BRONJ, which is influenced by factors such as dental diseases, invasive dental procedures, and poor oral hygiene [39–42]. Infection and inflammation play crucial roles in the development of BRONJ [43], involving various immune cells and leading to a deterioration of the bone-immune microenvironment [44]. Previous studies have primarily focused on osteoclast differentiation and maturation, angiogenesis, and osteogenesis as approaches to prevent and treat BRONJ using diverse biomaterials such as tetrahedral framework nucleic acid, borate bioactive glass, and platelet-derived growth factor [22,45–47]. Given the clinical significance of BRONJ and the immunoregulatory function of macrophages, our study aimed to develop a thermosensitive hydrogel loaded with Ce-MBGNs and ApoEVs to treat BRONJ. This novel formulation was designed to regulate macrophage polarization and prevent bone necrosis caused by BPs. Our findings indicate that this formulation can recruit and rescue macrophages from the detrimental effects of ZA. Moreover, it can induce a shift in macrophage phenotype from M1 to M2, both in vitro and in vivo. This shift promotes the resolution of inflammation, reduces necrotic bone formation, and accelerates bone regeneration in the context of BRONJ. These results highlight the potential of the developed Ce-MBGNs and ApoEVs-loaded hydrogel as a promising therapeutic approach for alleviating BRONJ.

Inspired by marine mussels, chitosan hydrogel modified by the catechol functional group has been reported to be capable of adhering to various wet surfaces [38]. Additionally, pluronic F-127 copolymers are known for their ability to undergo reversible sol-gel transition in response to changes in temperature [38]. Therefore, we utilized CH/PF hydrogel to deliver ApoEVs and Ce-MBGNs to treat BRONJ. Ce-MBGNs have been widely used in wound healing, tissue engineering, and other fields due to their antibacterial, anti-inflammatory, osteogenic, and antioxidant properties [24–26,48,49]. Previous studies have demonstrated that Ce-MBGNs can reduce M1 polarization and promote M2 polarization of macrophages, thus effectively eliminating inflammation [25,26]. Macrophages play a crucial role in the innate immune response and are involved in various stages of wound healing processes. M1 macrophages are pro-inflammatory cells capable of killing pathogens, while M2 macrophages are anti-inflammatory cells that promote tissue repair. ZA has been found to promote M1 macrophage polarization via a TLR-4-mediated pathway in BRONJ [14]. In our study, the results from cell immunofluorescence, WB, and qRT-PCR demonstrate an increase in M1 polarization marker expression (CD86, iNOS, TNF-α, and IL-6) and a decrease in M2 polarization marker expression (CD206, Arginase1, TGF-β1, and IL-10) in the ZA group. This suggests that ZA promotes M1 polarization and inhibits M2 polarization. However, Ce-MBGNs have the opposite effect and can restore the polarization level to that of the control group. This finding is consistent with previous studies [25,26]. Reactive oxygen species (ROS) are oxygen-free radicals produced during oxidation reactions that play various physiological roles in different biological processes [50,51]. ROS production is crucial for macrophage activation and the pro-inflammatory state [51–53]. Ce can scavenge ROS and regulate oxygen levels in the microenvironment through its oxidation states (Ce^{4+} and Ce^{3+}) [23,25,26]. Additionally, low ROS levels have been shown to be favorable for M2 polarization [53,54]. Therefore, the ability of Ce-MBGNs to promote M2 macrophage polarization can be attributed to their ROS scavenging properties.

The PI3K/Akt pathway is known to play a crucial role in macrophage polarization, influencing various cellular processes such as energy metabolism, redox status, lipid metabolism, and the production of inflammatory factors [55–57]. It ultimately regulates the functionality and immune responses of macrophages. When exposed to LPS, macrophages undergo M1 polarization by activating the AKT/mTOR pathway via the TLR4 receptor [58–60]. However, the specific role of ZA in this process has not yet been fully elucidated. Our findings suggest that ZA can activate the PI3K/Akt pathway. Interestingly, recent studies have shown that Ce, known for its reactive oxygen species scavenging activity, can inhibit the PI3K/AKT pathway [61,62]. Our study further confirmed that Ce-MBGNs could indeed inhibit the activation of the PI3K/AKT pathway induced by ZA. The WB results and their quantitative analysis (Fig. 4F) demonstrated that ZA stimulation significantly increased Akt and mTOR phosphorylation compared to the blank control. In contrast, the hydrogels alone and the hydrogels + ApoEVs groups did not show increased Akt and mTOR phosphorylation. When ApoEVs were combined with ZA, Akt and mTOR phosphorylation were increased, although slightly less than with ZA alone. Notably, the Hydrogel + ZA + Ce-MBGNs + ApoEVs group did not increase Akt and mTOR phosphorylation compared to the blank control. These findings suggest that Ce-MBGNs may inhibit the activation of the PI3K/Akt/mTOR signaling pathway induced by ZA, as only the groups containing ZA showed increased Akt and mTOR phosphorylation.

ApoEVs, extracellular vesicles derived from dying cells, can be produced by various cell types, including stem cells, immune cells, osteoblasts, and endothelial cells [63]. During apoptosis, dying cells release "find me" signals, which are molecular factors that attract phagocytes [64,65]. Similarly, ApoEVs possess chemotactic properties and can recruit phagocytes. For instance, microparticles derived from apoptotic cells, carrying intercellular adhesion molecule 3, have been found to promote macrophage chemoattraction [66]. Studies have demonstrated that apoptotic cells release abundant extracellular vesicles that can stimulate macrophages to produce TGF in vivo and in vitro [67]. ApoEVs also inhibit macrophages from adopting a pro-inflammatory phenotype through the AMPK/SIRT1/NF-κB pathway and suppress the formation of adjacent osteoclasts by reducing TNF-α secretion [68]. These findings suggest that ApoEVs play a role in modulating macrophage behavior and inflammation response.

In our study, we compared ApoEVs derived from different cell lines, including MC3T3, VECs, LECs, and L929, to identify the ApoEVs with the strongest macrophage recruitment capacity (Fig. 3). Interestingly, ApoEVs derived from MC3T3 cells exhibited the highest ability to promote macrophage migration, as shown in Fig. 3A. Moreover, the phagocytosis assay demonstrated that macrophages were capable of engulfing ApoEVs derived from MC3T3 cells, as depicted in Fig. 3C. By leveraging the macrophage recruitment capacity of ApoEVs and the macrophage polarization capacity of Ce-MBGNs, we can enhance the recruitment of macrophages to the affected area, and subsequently stimulate the resolution of inflammation through M2 polarization and facilitate tissue repair in cases of BRONJ. This approach of combining ApoEVs and Ce-MBGNs holds the potential for promoting effective healing and regeneration in BRONJ patients.

To overcome the challenges posed by the oral environment and enhance the ease of use in clinical applications, a suitable carrier is required to load ApoEVs and Ce-MBGNs. The wound in BRONJ patients is often exposed to saliva and chewing, making it necessary to develop a carrier that can resist adverse effects while maintaining operability. In this regard, we were inspired by the adhesive properties of marine mussels and utilized catechol-functionalized chitosan, along with PF-127, to create an injectable thermosensitive adhesive hydrogel. The modified chitosan was designed to enable sustained and stable release of ApoEVs and Ce-MBGNs. Previous studies have shown that a mixture of catechol-conjugated chitosan and thiolated Pluronic F-127 can transform from a viscous solution state at room temperature to a cross-linked gel state at body temperature [38]. This hydrogel can strongly adhere to soft tissues even in the presence of mucous layers, making it an ideal candidate as a carrier for ApoEVs and Ce-MBGNs in a challenging oral environment.

The rheological analysis revealed that the hydrogel could undergo gelling at a temperature of approximately 30°C, and the presence of MBGNs or Ce-MBGNs had no significant impact on gel formation (as shown in Fig. 1). In vitro degradation tests were conducted to assess the degradation behaviors of CHI, CH/PF, MBGNs, and Ce-MBGNs. It was observed that CHI and CH/PF could retain mass up to ~60 % after immersion in lysozyme-containing DPBS for 21 d, while in the presence of MBGNs or Ce-MBGNs, the remaining mass of the hydrogels increased to ~73 %. This lower mass loss in the MBGNs and Ce-MBGNs groups may be attributed to the ion release from nanoparticles, which could enhance the cross-linkage of CH/PF. However, all hydrogel formulations could fully degrade within 4 weeks in vivo as indicated by the HE staining results. In the ion release test, it was observed that both MBGNs and Ce-MBGNs could slowly release Ca and Si ions when incorporated into the hydrogel. However, the amount of Ca ions released by the Ce-MBGNs group was smaller compared to the MBGNs group. This difference may be attributed to the lower CaO concentration in the Ce-MBGNs framework, as indicated in our previous study [26]. On the other hand, no Ce ions were detected from the Ce-MBGNs group, probably due to the low concentration of Ce ions released from CH/PF + Ce-MBGNs exceeding the detection limit. A similar phenomenon has been observed in our previous study [26]. In addition, Ce ions tend to form insoluble complexes in the presence of phosphate groups rather than dissolving into the solution [69], which could also cause the non-detection of Ce ions. ApoEVs could also be released in a sustained manner. Overall, these findings suggest that the hydrogel formulation has promising characteristics for use as a carrier for ApoEVs and Ce-MBGNs in BRONJ treatment.

We evaluated the effects of the hydrogel formulation on BRONJ. In the in vivo test illustrated in Fig. 5, our experimental groups included

control (blank control), ZA alone, hydrogel + ZA, hydrogel + ZA + Ce-MBGNs, and hydrogel + ZA + Ce-MBGNs + ApoEVs to investigate the synergistic effects of Ce-MBGNs and ApoEVs in alleviating BRONJ. ZA was intentionally included in all groups to establish the BRONJ model. The outcomes clearly demonstrated the beneficial impact of Ce-MBGNs on BRONJ alleviation. However, we acknowledge that the absence of the hydrogel + ZA + ApoEVs group might lead to confusion regarding the in vivo effects of ApoEVs on BRONJ alleviation. This absence limits a comprehensive understanding of the in vivo alleviation potential of ApoEVs for BRONJ. Nevertheless, our in vitro findings (Fig. 4) have already confirmed the regulatory effects of ApoEVs on macrophages, indicating their anti-inflammatory and recruitment properties, which suggest a positive role in BRONJ alleviation. Significantly, through a comparative analysis between the hydrogel + ZA + Ce-MBGNs and hydrogel + ZA + Ce-MBGNs + ApoEVs groups, we deduced that the presence of ApoEVs enhanced the alleviation effect compared to Ce-MBGNs alone on BRONJ. Combining Ce-MBGNs and ApoEVs exhibited synergistic effects, promoting extraction socket healing, reduced necrotic bone formation, and facilitated macrophage M2 phenotype polarization.

5. Conclusions

This study aimed to develop a novel approach to treat BRONJ by regulating the recruitment and polarization of macrophages through the use of Ce-MBGNs and ApoEVs loaded CH/PF hydrogels. The addition of 1 wt % Ce-MBGNs did not significantly affect the degradation, gelation, or rheological behavior of the catechol-conjugated chitosan-based hydrogels. Furthermore, the incorporation of 1 mg/mL ApoEVs in the hydrogels enhanced the migration of macrophages, while the presence of Ce-MBGNs promoted macrophage polarization towards the M2 phenotype. In vivo experiments performed on BRONJ mice revealed that the synergistic effects of Ce-MBGNs and ApoEVs led to increased macrophage recruitment, M2 polarization, and decreased M1 polarization. The composite hydrogels also facilitated mucosal and bone healing, resulting in alleviated jaw osteonecrosis. Overall, our findings provide a novel strategy for alleviating BRONJ through targeted immunomodulation. Catechol-conjugated chitosan-based hydrogels loaded with Ce-MBGNs and ApoEVs demonstrate great potential in this regard.

CRediT authorship contribution statement

Ziji Ling: Writing – review & editing, Writing – original draft, Visualization, Methodology, Investigation, Formal analysis, Data curation. **Songsong Guo:** Writing – original draft, Investigation, Formal analysis, Data curation. **Hanyu Xie:** Methodology, Investigation, Data curation. **Xinyu Chen:** Investigation. **Kui Yu:** Writing – review & editing, Investigation. **Hongbing Jiang:** Supervision, Resources, Project administration. **Rongyao Xu:** Supervision, Resources, Project administration, Conceptualization. **Yunong Wu:** Writing – review & editing, Supervision, Resources, Project administration. **Kai Zheng:** Writing – review & editing, Writing – original draft, Validation, Supervision, Resources, Project administration, Methodology, Funding acquisition, Formal analysis, Conceptualization.

Declaration of competing interest

The authors declare that they have no known competing financial interests or personal relationships that could have appeared to influence the work reported in this paper.

Data availability

Data will be made available on request.

Acknowledgments

This work was supported by the National Natural Science Foundation of China (No. 82101071 and 81771092), the Natural Science Foundation of Jiangsu Province (No. BK20210528), and the Opening Project Foundation of Jiangsu Province Key Laboratory of Oral Diseases (JSKLOD-KF-2104).

References

[1] S.L. Ruggiero, T.B. Dodson, L.A. Assael, R. Landesberg, R.E. Marx, B. Mehrotra, American association of oral and maxillofacial surgeons position paper on bisphosphonate-related osteonecrosis of the jaws–2009 update, J. Oral Maxillofac. Surg. 67 (2009) 2–12.
[2] E.A. Sigua-Rodriguez, R. da Costa Ribeiro, A.C. de Brito, N. Alvarez-Pinzon, J.R. de Albergaria-Barbosa, Bisphosphonate-related osteonecrosis of the jaw: a review of the literature, Int. J. Dent. (2014) 192320, 2014.
[3] E. Boopathi, R. Birbe, S.A. Shoyele, R.B. Den, C. Thangavel, Bone health management in the continuum of prostate cancer disease, Cancers. (Basel) 14 (2022).
[4] A. Göbel, R.M. Riffel, L.C. Hofbauer, T.D. Rachner, The mevalonate pathway in breast cancer biology, Cancer Lett. 542 (2022) 215761.
[5] M. Hussain, F. Khan, S. Al Hadidi, The use of bone-modifying agents in multiple myeloma, Blood Rev. (2022) 100999.
[6] E.M. Rabjohns, K. Hurst, A. Ghosh, M.C. Cuellar, R.R. Rampersad, T.K. Tarrant, Paget's Disease of Bone: Osteoimmunology and Osteoclast Pathology, Curr. Allergy Asthma Rep. 21 (2021) 23.
[7] S. Song, Y. Guo, Y. Yang, D. Fu, Advances in pathogenesis and therapeutic strategies for osteoporosis, Pharmacol. Ther. 237 (2022) 108168.
[8] A.C. van der Burgh, C.E. de Keyser, M.C. Zillikens, B.H. Stricker, The Effects of Osteoporotic and Non-osteoporotic Medications on Fracture Risk and Bone Mineral Density, Drugs 81 (2021) 1831–1858.
[9] N.H. Beth-Tasdogan, B. Mayer, H. Hussein, O. Zolk, J.U. Peter, Interventions for managing medication-related osteonecrosis of the jaw, Cochrane Database Syst. Rev. 7 (2022) Cd012432.
[10] S.W. On, S.W. Cho, S.H. Byun, B.E. Yang, Various Therapeutic Methods for the Treatment of Medication-Related Osteonecrosis of the Jaw (MRONJ) and Their Limitations: A Narrative Review on New Molecular and Cellular Therapeutic Approaches, Antioxidants. (Basel) 10 (2021).
[11] E.B. Bermúdez-Bejarano, M. Serrera-Figallo, A. Gutiérrez-Corrales, M.M. Romero-Ruiz, R. Castillo-de-Oyagüe, J.L. Gutiérrez-Pérez, D. Torres-Lagares, Prophylaxis and antibiotic therapy in management protocols of patients treated with oral and intravenous bisphosphonates, J. Clin. Exp. Dent. 9 (2017) e141–e149.
[12] F. Hallmer, T. Bjørnland, G. Andersson, J.P. Becktor, A.K. Kristoffersen, M. Enersen, Bacterial diversity in medication-related osteonecrosis of the jaw, Oral Surg. Oral Med. Oral Pathol. Oral Radiol. 123 (2017) 436–444.
[13] P. Paschalidi, I. Gkouveris, A. Soundia, E. Kalfarentzos, E. Vardas, M. Georgaki, G. Kostakis, B.M. Erovic, S. Tetradis, C. Perisanidis, N.G. Nikitakis, The role of M1 and M2 macrophage polarization in progression of medication-related osteonecrosis of the jaw, Clin. Oral Investig. 25 (2021) 2845–2857.
[14] W. Zhu, R. Xu, J. Du, Y. Fu, S. Li, P. Zhang, L. Liu, H. Jiang, Zoledronic acid promotes TLR-4-mediated M1 macrophage polarization in bisphosphonate-related osteonecrosis of the jaw, FASEB J. 33 (2019) 5208–5219.
[15] A. Hoppe, N.S. Güldal, A.R. Boccaccini, A review of the biological response to ionic dissolution products from bioactive glasses and glass-ceramics, Biomaterials 32 (2011) 2757–2774.
[16] M. Vallet-Regí, E. Ruiz-Hernández, Bioceramics: from bone regeneration to cancer nanomedicine, Adv. Mater. 23 (2011) 5177–5218.
[17] M. Vallet-Regi, A.J. Salinas, Mesoporous bioactive glasses for regenerative medicine, Mater. Today Bio 11 (2021) 100121.
[18] S. Kargozar, M. Mozafari, S. Ghodrat, E. Fiume, F. Baino, Copper-containing bioactive glasses and glass-ceramics: From tissue regeneration to cancer therapeutic strategies, Mater. Sci. Eng. C. Mater. Biol. Appl. 121 (2021) 111741.
[19] K. Zheng, B. Sui, K. Ilyas, A.R. Boccaccini, Porous bioactive glass micro- and nanospheres with controlled morphology: developments, properties and emerging biomedical applications, Mater. Horiz. 8 (2021) 300–335.
[20] S. Kargozar, F. Baino, S. Hamzehlou, R.G. Hill, M. Mozafari, Bioactive glasses entering the mainstream, Drug Discov. Today 23 (2018) 1700–1704.
[21] C. Wu, J. Chang, Multifunctional mesoporous bioactive glasses for effective delivery of therapeutic ions and drug/growth factors, J. Control Release 193 (2014) 282–295.
[22] Z. Su, J. Li, X. Bai, F.R. Tay, M. Zhang, K. Liang, L. He, H. Yuan, J. Li, Borate bioactive glass prevents zoledronate-induced osteonecrosis of the jaw by restoring osteogenesis and angiogenesis, Oral Dis. 26 (2020) 1706–1717.
[23] S.M. Hirst, A.S. Karakoti, R.D. Tyler, N. Sriranganathan, S. Seal, C.M. Reilly, Anti-inflammatory properties of cerium oxide nanoparticles, Small. 5 (2009) 2848–2856.
[24] A. Zambon, G. Malavasi, A. Pallini, F. Fraulini, G. Lusvardi, Cerium Containing Bioactive Glasses: A Review, ACS. Biomater. Sci. Eng. 7 (2021) 4388–4401.
[25] F. Kurtuldu, H. Kaňková, A.M. Beltrán, L. Liverani, D. Galusek, A.R. Boccaccini, Anti-inflammatory and antibacterial activities of cerium-containing mesoporous bioactive glass nanoparticles for drug-free biomedical applications, Mater. Today Bio 12 (2021) 100150.

[26] K. Zheng, E. Torre, A. Bari, N. Taccardi, C. Cassinelli, M. Morra, S. Fiorilli, C. Vitale-Brovarone, G. Iviglia, A.R. Boccaccini, Antioxidant mesoporous Ce-doped bioactive glass nanoparticles with anti-inflammatory and pro-osteogenic activities, Mater. Today Bio 5 (2020) 100041.
[27] Y. Sun, X. Sun, X. Li, W. Li, C. Li, Y. Zhou, L. Wang, B. Dong, A versatile nanocomposite based on nanoceria for antibacterial enhancement and protection from aPDT-aggravated inflammation via modulation of macrophage polarization, Biomaterials 268 (2021) 120614.
[28] I.K. Poon, Y.H. Chiu, A.J. Armstrong, J.M. Kinchen, I.J. Juncadella, D.A. Bayliss, K. S. Ravichandran, Unexpected link between an antibiotic, pannexin channels and apoptosis, Nature 507 (2014) 329–334.
[29] G.K. Atkin-Smith, R. Tixeira, S. Paone, S. Mathivanan, C. Collins, M. Liem, K. J. Goodall, K.S. Ravichandran, M.D. Hulett, I.K. Poon, A novel mechanism of generating extracellular vesicles during apoptosis via a beads-on-a-string membrane structure, Nat. Commun. 6 (2015) 7439.
[30] I.K.H. Poon, M.A.F. Parkes, L. Jiang, G.K. Atkin-Smith, R. Tixeira, C.D. Gregory, D. C. Ozkocak, S.F. Rutter, S. Caruso, J.P. Santavanond, S. Paone, B. Shi, A.L. Hodge, M.D. Hulett, J.D.Y. Chow, T.K. Phan, A.A. Baxter, Moving beyond size and phosphatidylserine exposure: evidence for a diversity of apoptotic cell-derived extracellular vesicles in vitro, J. ExtraCell Vesicles. 8 (2019) 1608786.
[31] S. Caruso, I.K.H. Poon, Apoptotic Cell-Derived Extracellular Vesicles: More Than Just Debris, Front. Immunol. 9 (2018) 1486.
[32] A. Eguchi, A. Mulya, M. Lazic, D. Radhakrishnan, M.P. Berk, D. Povero, A. Gornicka, A.E. Feldstein, Microparticles release by adipocytes act as "find-me" signals to promote macrophage migration, PLoS. One 10 (2015) e0123110.
[33] M. Ghahremani Piraghaj, S. Soudi, H. Ghanbarian, Z. Bolandi, S. Namaki, S. M. Hashemi, Effect of efferocytosis of apoptotic mesenchymal stem cells (MSCs) on C57BL/6 peritoneal macrophages function, Life Sci. 212 (2018) 203–212.
[34] C. Zheng, B. Sui, X. Zhang, J. Hu, J. Chen, J. Liu, D. Wu, Q. Ye, L. Xiang, X. Qiu, S. Liu, Z. Deng, J. Zhou, S. Liu, S. Shi, Y. Jin, Apoptotic vesicles restore liver macrophage homeostasis to counteract type 2 diabetes, J. ExtraCell Vesicles. 10 (2021) e12109.
[35] S. Hoefert, C.Sade Hoefert, A. Munz, H. Northoff, A. Yuan, K. Reichenmiller, S. Reinert, M. Grimm, Altered macrophagic THP-1 cell phagocytosis and migration in bisphosphonate-related osteonecrosis of the jaw (BRONJ), Clin. Oral Investig. 20 (2016) 1043–1054.
[36] I. Gkouveris, A. Soundia, P. Gouveris, D. Zouki, D. Hadaya, S. Tetradis, Macrophage Involvement in Medication-Related Osteonecrosis of the Jaw (MRONJ): A Comprehensive, Short Review, Cancers. (Basel) 14 (2022).
[37] J.H. Ryu, S. Hong, H. Lee, Bio-inspired adhesive catechol-conjugated chitosan for biomedical applications: A mini review, Acta Biomater. 27 (2015) 101–115.
[38] J.H. Ryu, Y. Lee, W.H. Kong, T.G. Kim, T.G. Park, H. Lee, Catechol-functionalized chitosan/pluronic hydrogels for tissue adhesives and hemostatic materials, Biomacromolecules. 12 (2011) 2653–2659.
[39] C.H. Van Poznak, J.M. Unger, A.K. Darke, C. Moinpour, R.A. Bagramian, M. M. Schubert, L.K. Hansen, J.D. Floyd, S.R. Dakhil, D.L. Lew, J.L. Wade, 3rd, M. J. Fisch, N.L. Henry, D.L. Hershman, J. Gralow, Association of Osteonecrosis of the Jaw With Zoledronic Acid Treatment for Bone Metastases in Patients With Cancer, JAMa Oncol. 7 (2021) 246–254.
[40] J. Everts-Graber, D. Lehmann, J.P. Burkard, B. Schaller, B. Gahl, H. Häuselmann, U. Studer, H.R. Ziswiler, S. Reichenbach, T. Lehmann, Risk of Osteonecrosis of the Jaw Under Denosumab Compared to Bisphosphonates in Patients With Osteoporosis, J. Bone Miner. Res. 37 (2022) 340–348.
[41] K. McGowan, T. McGowan, S. Ivanovski, Risk factors for medication-related osteonecrosis of the jaws: A systematic review, Oral Dis. 24 (2018) 527–536.
[42] S.L. Ruggiero, T.B. Dodson, T. Aghaloo, E.R. Carlson, B.B. Ward, D. Kademani, American Association of Oral and Maxillofacial Surgeons' Position Paper on Medication-Related Osteonecrosis of the Jaws-2022 Update, J. Oral Maxillofac. Surg. 80 (2022) 920–943.
[43] A.A. Khan, A. Morrison, D.A. Hanley, D. Felsenberg, L.K. McCauley, F. O'Ryan, I. R. Reid, S.L. Ruggiero, A. Taguchi, S. Tetradis, N.B. Watts, M.L. Brandi, E. Peters, T. Guise, R. Eastell, A.M. Cheung, S.N. Morin, B. Masri, C. Cooper, S.L. Morgan, B. Obermayer-Pietsch, B.L. Langdahl, R. Al Dabagh, K.S. Davison, D.L. Kendler, G. K. Sándor, R.G. Josse, M. Bhandari, M. El Rabbany, D.D. Pierroz, R. Sulimani, D. P. Saunders, J.P. Brown, J. Compston, Diagnosis and management of osteonecrosis of the jaw: a systematic review and international consensus, J. Bone Miner. Res. 30 (2015) 3–23.
[44] J. Chang, A.E. Hakam, L.K. McCauley, Current Understanding of the Pathophysiology of Osteonecrosis of the Jaw, Curr. Osteoporos. Rep. 16 (2018) 584–595.
[45] S.Y. Gao, R.B. Lin, S.H. Huang, Y.J. Liang, X. Li, S.E. Zhang, D.Q. Ouyang, K. Li, G. S. Zheng, G.Q. Liao, PDGF-BB exhibited therapeutic effects on rat model of bisphosphonate-related osteonecrosis of the jaw by enhancing angiogenesis and osteogenesis, Bone 144 (2021) 115117.
[46] D. Zhao, W. Cui, M. Liu, J. Li, Y. Sun, S. Shi, S. Lin, Y. Lin, Tetrahedral Framework Nucleic Acid Promotes the Treatment of Bisphosphonate-Related Osteonecrosis of the Jaws by Promoting Angiogenesis and M2 Polarization, ACS. Appl. Mater. Interfaces. 12 (2020) 44508–44522.
[47] D. Zhao, D. Xiao, M. Liu, J. Li, S. Peng, Q. He, Y. Sun, J. Xiao, Y. Lin, Tetrahedral framework nucleic acid carrying angiogenic peptide prevents bisphosphonate-related osteonecrosis of the jaw by promoting angiogenesis, Int. J. Oral Sci. 14 (2022) 23.
[48] I. Atkinson, A.M. Seciu-Grama, S. Petrescu, D. Culita, O.C. Mocioiu, M. Voicescu, R. A. Mitran, D. Lincu, A.M. Prelipcean, O. Craciunescu, Cerium-Containing Mesoporous Bioactive Glasses (MBGs)-Derived Scaffolds with Drug Delivery Capability for Potential Tissue Engineering Applications, Pharmaceutics. 14 (2022).
[49] F. Westhauser, F. Rehder, S. Decker, E. Kunisch, A. Moghaddam, K. Zheng, A. R. Boccaccini, Ionic dissolution products of Cerium-doped bioactive glass nanoparticles promote cellular osteogenic differentiation and extracellular matrix formation of human bone marrow derived mesenchymal stromal cells, Biomed. Mater. 16 (2021).
[50] B. Kalyanaraman, Teaching the basics of redox biology to medical and graduate students: Oxidants, antioxidants and disease mechanisms, Redox. Biol. 1 (2013) 244–257.
[51] A. Covarrubias, V. Byles, T. Horng, ROS sets the stage for macrophage differentiation, Cell Res. 23 (2013) 984–985.
[52] E.L. Mills, B. Kelly, A. Logan, A.S.H. Costa, M. Varma, C.E. Bryant, P. Tourlomousis, J.H.M. Däbritz, E. Gottlieb, I. Latorre, S.C. Corr, G. McManus, D. Ryan, H.T. Jacobs, M. Szibor, R.J. Xavier, T. Braun, C. Frezza, M.P. Murphy, L.A. O'Neill, Succinate Dehydrogenase Supports Metabolic Repurposing of Mitochondria to Drive Inflammatory Macrophages, Cell 167 (2016) 457–470, e13.
[53] H.Y. Tan, N. Wang, S. Li, M. Hong, X. Wang, Y. Feng, The Reactive Oxygen Species in Macrophage Polarization: Reflecting Its Dual Role in Progression and Treatment of Human Diseases, Oxid. Med. Cell Longev. 2016 (2016) 2795090.
[54] J. Kim, H.Y. Kim, S.Y. Song, S.H. Go, H.S. Sohn, S. Baik, M. Soh, K. Kim, D. Kim, H. C. Kim, N. Lee, B.S. Kim, T. Hyeon, Synergistic Oxygen Generation and Reactive Oxygen Species Scavenging by Manganese Ferrite/Ceria Co-decorated Nanoparticles for Rheumatoid Arthritis Treatment, ACS. Nano 13 (2019) 3206–3217.
[55] J. Li, B. Diao, S. Guo, X. Huang, C. Yang, Z. Feng, W. Yan, Q. Ning, L. Zheng, Y. Chen, Y. Wu, VSIG4 inhibits pro-inflammatory macrophage activation by reprogramming mitochondrial pyruvate metabolism, Nat. Commun. 8 (2017) 1322.
[56] R.A. Pengal, L.P. Ganesan, G. Wei, H. Fang, M.C. Ostrowski, S. Tridandapani, Lipopolysaccharide-induced production of interleukin-10 is promoted by the serine/threonine kinase Akt, Mol. Immunol. 43 (2006) 1557–1564.
[57] V. Byles, A.J. Covarrubias, I. Ben-Sahra, D.W. Lamming, D.M. Sabatini, B. D. Manning, T. Horng, The TSC-mTOR pathway regulates macrophage polarization, Nat. Commun. 4 (2013) 2834.
[58] V. Schaeffer, S. Arbabi, I.A. Garcia, M.L. Knoll, J. Cuschieri, E.M. Bulger, R. V. Maier, Role of the mTOR pathway in LPS-activated monocytes: influence of hypertonic saline, J. Surg. Res. 171 (2011) 769–776.
[59] Y.J. Kim, J. Jin, D.H. Kim, D. Kim, Y.M. Lee, J.K. Byun, Y.K. Choi, K.G. Park, SGLT2 inhibitors prevent LPS-induced M1 macrophage polarization and alleviate inflammatory bowel disease by downregulating NHE1 expression, Inflam. Research 72 (2023) 1981–1997.
[60] B.W. Jones, K.A. Heldwein, T.K. Means, J.J. Saukkonen, M.J. Fenton, Differential roles of Toll-like receptors in the elicitation of pro-inflammatory responses by macrophages, Ann. Rheum. Dis. 60 (3) (2001) iii6–ii12. Suppl.
[61] S. Bao, D. Yu, Z. Tang, H. Wu, H. Zhang, N. Wang, Y. Liu, H. Huang, C. Liu, X. Li, Z. Guo, Conformationally regulated "nanozyme-like" cerium oxide with multiple free radical scavenging activities for osteoimmunology modulation and vascularized osseointegration, Bioact. Mater. 34 (2024) 64–79.
[62] M. Li, X. Chu, D. Wang, L. Jian, L. Liu, M. Yao, D. Zhang, Y. Zheng, X. Liu, Y. Zhang, F. Peng, Tuning the surface potential to reprogram immune microenvironment for bone regeneration, Biomaterials 282 (2022) 121408.
[63] L. Jiang, S. Paone, S. Caruso, G.K. Atkin-Smith, T.K. Phan, M.D. Hulett, I.K.H. Poon, Determining the contents and cell origins of apoptotic bodies by flow cytometry, Sci. Rep. 7 (2017) 14444.
[64] A. Hochreiter-Hufford, K.S. Ravichandran, Clearing the dead: apoptotic cell sensing, recognition, engulfment, and digestion, Cold. Spring. Harb. Perspect. Biol. 5 (2013) a008748.
[65] L. Zitvogel, O. Kepp, G. Kroemer, Decoding cell death signals in inflammation and immunity, Cell 140 (2010) 798–804.
[66] E.E. Torr, D.H. Gardner, L. Thomas, D.M. Goodall, A. Bielemeier, R. Willetts, H. R. Griffiths, L.J. Marshall, A. Devitt, Apoptotic cell-derived ICAM-3 promotes both macrophage chemoattraction to and tethering of apoptotic cells, Cell Death. Differ. 19 (2012) 671–679.
[67] H. Chen, S. Kasagi, C. Chia, D. Zhang, E. Tu, R. Wu, P. Zanvit, N. Goldberg, W. Jin, W. Chen, Extracellular Vesicles from Apoptotic Cells Promote TGFβ Production in Macrophages and Suppress Experimental Colitis, Sci. Rep. 9 (2019) 5875.
[68] Q. Ye, H. Xu, S. Liu, Z. Li, J. Zhou, F. Ding, X. Zhang, Y. Wang, Y. Jin, Q. Wang, Apoptotic extracellular vesicles alleviate Pg-LPS induced inflammation of macrophages via AMPK/SIRT1/NF-κB pathway and inhibit adjacent osteoclast formation, J. Periodontol. (2022).
[69] S. Shruti, A.J. Salinas, G. Malavasi, G. Lusvardi, L. Menabue, C. Ferrara, P. Mustarelli, M. Vallet-Regì, Structural and in vitro study of cerium, gallium and zinc containing sol–gel bioactive glasses, J. Mater. Chem. 22 (2012) 13698–13706.